ACS APPLIED MATERIALS & INTERFACES

Research Article

www.acsami.org

Scalable and Versatile Graphene Functionalized with the Mannich Condensate

Ruijuan Liao,[†] Zhenghai Tang,[†] Tengfei Lin,[†] and Baochun Guo*[,†,‡]

[†]Department of Polymer Materials and Engineering, South China University of Technology, Guangzhou, 510640, P. R. China

[‡]State Key Laboratory of Pulp and Paper Engineering, South China University of Technology, Guangzhou, 510640, P. R. China

ABSTRACT: The functionalized graphene (JTPG) is fabricated by chemical conversion of graphene oxide (GO), using tea polyphenols (TP) as the reducer and stabilizer, followed by further derivatization through the Mannich reaction between the pyrogallol groups on TP and Jeffamine M-2070. JTPG exhibits solubility in a broad spectrum of solvents, long-term stability and single-layered dispersion in water and organic solvents, which are substantiated by AFM, TEM, and XRD. The paper-like JTPG hybrids prepared by vacuum-assisted filtration exhibits an unusual combination of high toughness (tensile strength of ~275 MPa and break strain of ~8%) and high electrical conductivity (~700 S/m). Still, JTPG is revealed to be very promising in the fabrication of polymer/graphene composites due to the excellent solubility in the solvent with low boiling point and low toxicity. Accordingly, as an example, nitrile rubber/JTPG composites are fabricated by the solution compounding in acetone. The resulted composite shows low threshold percolation at 0.23 vol.% of graphene. The versatilities both in dispersibility and performance, together with the scalable process of JTPG, enable a new way to scale up the fabrication of the graphene-based polymer composites or hybrids with high performance.

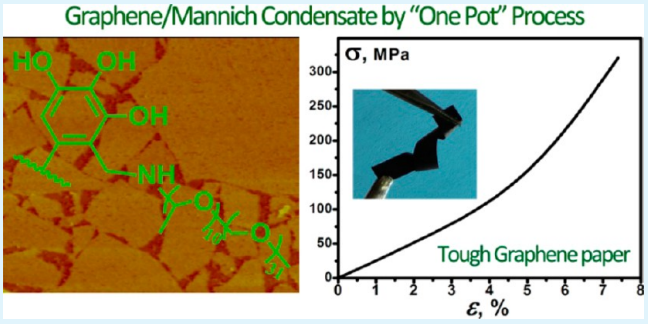

KEYWORDS: *graphene, Mannich condensation, solubility, polyphenols, polymer composite*

INTRODUCTION

As the thinnest material in the world, graphene has attracted tremendous interest owning to its intriguing and unparalleled physical properties.[1−5] Many investigations have been conducted to evaluate graphene's potential for improving the typical disadvantages of polymers such as low strength and low conductivity, by exploiting different polymer/graphene composites. To maximize the potential of graphene in a polymer-based composite, the single-layered and uniform dispersion in combination with suitable interfacial interaction between the graphene sheet and matrix is essential. However, such a goal has been considered to be difficult due to the low compatibility between graphene and polymer and strong van der Waals forces among the graphene layers.[6] Accordingly, the functionalization of graphene, aimed at improving the solubility in solvents or compatibility with polymer, is a must for the application of graphene in polymers. Among the preparation methods for graphene, the reduction of graphene oxide (GO) has been deemed to be a convenient and promising way to the mass production of graphene. The decoration methods have been divided broadly into two groups, namely covalent fashion and noncovalent fashion.[7] For example, graphene has been reported to be functionalized covalently by *p*-nitrobenediazonium,[8] poly-*L*-lysine,[9] functionalized porphyrin,[10] amine-terminated ionic liquid,[11] and 3-aminopropyltriethoxysilane[12] or noncovalently by 2D covalent organic framework,[13] bis(2,2′:6′,2″-terpyridine) metal-connected diblock copolymer,[14] biofunctional-modified poly(2-methoxystyrene),[15] poly(diallyldimethylammonium chloride),[16] 1-pyrenebutyrate,[17] fluorescent whitening agents,[18] Rhodamine B,[19] dendronized perylene bisimides,[20] graphitic carbon nitride polymer,[21] and sulfonated polyaniline.[22] Noticeably, most of the reported decorators for the graphene were toxic. More importantly, the functionalization processes were involved with the utilization of the organic solvents with high boiling point and toxicity. Still, these processes are not scalable due to the limitation in the concentration of graphene and the relatively long-term procedure. Consequently, the above-mentioned preparation processes are not suitable for mass production of the functionalized graphene. Therefore, the exploitation of the scalable process with a less complicated procedure is still of great importance for the application of the functionalized graphene in polymer composites.

Recently the present authors[23] and Shi et al.[24] conducted a simultaneous reduction and decoration of GO with tea polyphenols (TP), by which successful functionalization and promising performance of the reduced GO were obtained.[23] For better solubility and versatility of graphene by a facile process, in the present work, we performed Mannich condensation between the TP-reduced GO (TPG) and a

Received: December 29, 2012
Accepted: March 6, 2013
Published: March 6, 2013

   dx.doi.org/10.1021/am3032822 | *ACS Appl. Mater. Interfaces* 2013, 5, 2174−2181

commercially available polyetheramine, Jeffamine M-2070. A kind of functionalized graphene by Mannich condensate (JTPG) is accordingly formed. Due to the one-pot process in water, adoption of cheap and industrially available raw materials, the fabrication of JTPG could be easily scaled up. In the present paper, the attractive characteristics of JTPG, including solubility in broad spectrum of solvents, availability as slurry form, and stability have been revealed. The structure and performance of JTPG-based hybrid papers and the effectives of JTGP in the fabrication of polymer-based composites were presented and discussed.

EXPERIMENTAL SECTION

Raw Materials. Graphite powder (<20 mm) was purchased from Shanghai Colloidal Co. Ltd. Jeffamine M-2070 (M-2070), with an average molecular formula of [H_3C-(OCH_2CH_2)$_{31}$-(OCH_2CH-CH_3)$_{10}$-NH_2], was kindly supplied by Huntsman, USA. TP and epigallocatechin gallate (EGCG, purity of 99%) were purchased from Xuancheng Baicao Plant Co. Ltd., Anhui, China and Xi'an Haoxuan Biotechnology Ltd., Xi'an, China, respectively. Nitrile rubber (NBR) was purchased from Nandi Chemical Co. Ltd., Zhengjiang, China. The acrylonitrile content is 33 wt %. Other chemicals were analytically pure and used as received.

Production of Colloidal Suspension of JTPG. GO was prepared by oxidizing natural graphite according to a modified Hummer's method.[25] The TPG colloid was prepared by chemical reduction and modification of GO using TP according to our previous paper.[23] Typically, 0.3 g of TP is added to a GO aqueous solution (100 mL, 1 mg/mL) under sonication. The mixture is maintained at 80 °C for 4 h under constant stirring, and then the TPG colloid is obtained. Immediately, the sample of TPG was subjected to further derivatization as described below. The mixture of ethanol (30 mL), M-2070 (3.93 g), and formaldehyde (HCHO) is added to the TPG suspension, and the mixture is reacted under stirring at 80 °C for 1 h. After that, the suspension is cooled down to room temperature and subjected to centrifugation (14000 rpm) with plenty of water several times to remove the residual free M-2070. To investigate the Mannich reaction process, three parallel samples with the formaldehyde/amine molar ratio of 0, 0.33, and 1 were prepared, which were named as JTPG0, JTPG1, and JTPG2, respectively.

Production of J-EGCG. J-EGCG was used as the model substance to investigate the Mannich reaction mechanism between TP and Jeffamine M-2070. The preparation of J-EGCG, similar to that for JTPG2, is described as follows. EGCG (0.3 g) is dissolved in 300 mL of deionized water. The mixture of ethanol (30 mL), M-2070 (3.93 g), and HCHO (0.06 g) is then added to the EGCG solution, and the mixture is reacted under stirring at 80 °C for 1 h. After the subsequent lyophilization, J-EGCG is obtained and subjected to further characterizations.

Preparation of JTPG Papers. JTPG paper is made by vacuum-assisted filtration of the JTPG colloid, in which the free M-2070 is completely removed, through a nylon membrane filter (47 mm in diameter, 0.22 μm pore size), followed by peeling from the membrane. The papers are dried at 80 °C until equilibrium weight is achieved.

Preparation of JTPG/NBR Composite. A certain amount of JTPG2 is dispersed in acetone by sonication for 30 min at room temperature. NBR (20 g) was dissolved in acetone. Then, NBR solution is added into JTPG2 dispersion under consistent stirring. The mixing lasted for about 4 h. Dicumyl peroxide (0.1 g) is then added, and most of the acetone is evaporated. The mixture is further vacuum-dried at 40 °C for 12 h. Finally, the resulting compound is subjected to compression molding at 150 °C for 8 min.

Characterizations. *Characterizations for the Reaction between TPG and Jeffamine.* FTIR spectra were conducted on the JTPG papers using attenuated total reflectance mode with a Bruker Vertex 70 FTIR spectrometer. ^{1}H NMR spectroscopy was recorded on a Bruker MQ nuclear magnetic resonance spectrometer with a vibration frequency of 400 MHz. Gel permeation chromatography (GPC) analysis was conducted with a Agilent 1100 series. The molecular weight was obtained using polystyrenes as the standard and THF as the eluent at a flow rate of 1.0 mL/min at 30 °C. X-ray photoelectron spectroscopy (XPS) analysis was carried out on a Kratos Axis Ultra DLD with Al Kα radiation (1486.6 eV). UV−vis spectra of GO, Jeffamine, TPG, and JTPG aqueous solutions were collected on a Scinco S-3150 spectrometer. Thermogravimetric analysis (TGA) was performed under nitrogen atmosphere with a TA TGA Q5000 at a heating rate of 10 °C.min^{-1}.

Characterizations on the Dispersibility of JTPG, JTPG Papers, and NBR/JTGP Composites. Atomic force microscopy (AFM) was conducted on Veeco Multimode V operated in a tapping mode. The sample for AFM measurement was prepared by dispersing in water and drop-casting on a freshly cleaved mica surface. The mica was dried at ambient conditions for 24 h before the examination. Transmission electron microscope (TEM) image was obtained with a Philips Tecnai 12 TEM machine at an accelerating voltage of 30 kV. Scanning electron microscope (SEM) images were taken in a field emission scanning electron microscope (FESEM, Nova Nano SEM 430). X-ray diffraction (XRD) patterns were recorded using a Bruker D8 Advance X-ray diffractometer with Cu Kα radiation. Raman spectra were taken by LabRAM Aramis of HO RIBA Jobin Yovon, equipped with a He−Ne ion laser (632.8 nm) as excitation source. The electrical conductivity of all the samples was measured by a four-probe method on a Keithley 2365A instrument. The tensile strength of JTPG paper was determined on a tensile machine for fibers (YG004A, the Second textile machines Co. Ltd., Changzhou, China) at 25 °C and 75% relative humidity. All tensile tests were conducted in controlled strain mode with a preload of 0.1 cN, and the stretching rate was 1 mm·min^{-1}. The specimen was rectangular strips (1 mm × 30 mm). In order to ensure reliable and repeatable data, at least 30 quality specimens were used for each sample.

RESULTS AND DISCUSSION

Derivatization Process of TPG through Mannich Condensation. Previously, we have reported that TP is an effective reducing agent and stabilizer for graphene.[23] Subsequently, in virtue of the reactivity of the orthoquinones on oxidized TP, dodecylmercaptan was coupled onto the TPG by orthoquinone-thiol chemistry to enhance the organo-solubility of graphene.[23] Although the TPG and its derivative with thiol could be dispersed in water and some organic solvents, the solubility is still not satisfied, especially in the solvents with low boiling point and low toxicity. In the present work, aiming at further improved solubility and compatibility with various polymers, further derivatization of TPG was conducted by Mannich condensation between the surface phenols on TPG and a commercially available polyetheramine, Jeffamine M-2070. A series of derived TPG with M-2070 (JTPG) were obtained. As TP is a mixture of epicatechin (EC), epicatechin gallate (ECG), epigallocatechin (EGC), and epigallocatechin gallate (EGCG), in which EGCG is dominant (as high as 46 wt % of total TP),[26,27] we used EGCG as the model substance for the illustration of the process and characterization of the structure of JTPG. As schematically depicted in Scheme 1, EGCG is first oxidized to quinones during the reduction of GO, and then the quinones are self-condensated through phenolic coupling reactions to form polyphenol[28] (Scheme 1(a)). The formed polyphenols are the precursors for the Mannich reaction with M-2070. The Mannich condensation is schematically shown in Scheme 1 (b).

To substantiate the structure of JTPG as depicted in Scheme 1, FTIR, NMR, and GPC were conducted on JTPG and the model compound of J-EGCG. The FTIR spectra of JTPG with changing HCHO content are compared in Figure 1. For the three samples, the broad absorption around 3442 cm^{-1} is

Scheme 1. (a) Oxidation and Subsequent Coupling of EGCG and (b) Mannich Condensation between Phenols and M-2070

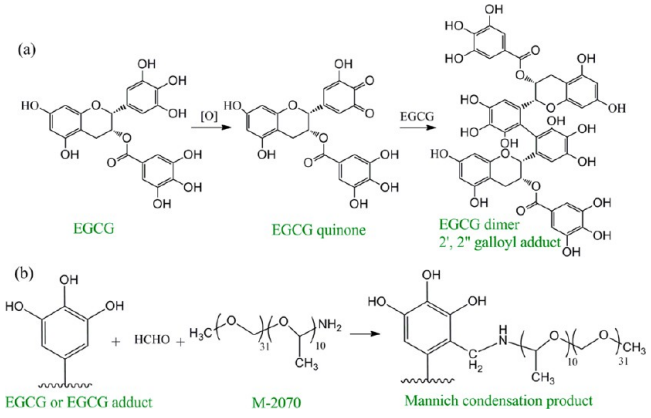

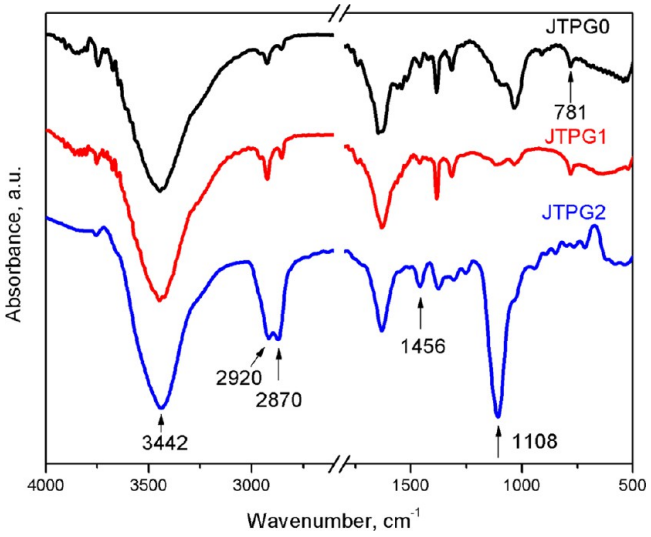

Figure 1. FTIR spectra of JTPG with consistently increasing HCHO dosage.

attributed to the overlaps of stretching vibrations of −OH from TP and −NH from M-2070. The peaks at 2920 and 2870 cm^{-1} are due to the antisymmetric and symmetric C−H stretching vibration of the $-CH_2-$ from M-2070 and the methylene bridged linkage between TP and M-2070. The peaks at 1456 and 1108 cm^{-1} are assigned to the N−H deformation vibration in-plane and the C−O stretching vibration from M-2070, respectively.[29] The increased intensities in the peaks around 1456 and 1108 cm^{-1} with consistently increasing HCHO dosage indicate the formation of Mannich condensate by the addition of HCHO. Further, noticeably, the peak around 781 cm^{-1}, characterizing the out-plane vibration of N−H for primary amine of M-2070, is not found in the FTIR spectrum of JTPG2, providing further implication of the Mannich condensation between the phenols on TPG and the amine of M-2070.

To further shed light on the Mannich condensation between TPG and M-2070, a model compound from the Mannich condensation between M-2070 and EGCG (J-EGCG) was prepared. The number-average molecular weight (Mn) of J-EGCG determined by GPC is about 65600 Da, which is largely increased compared with M-2070, implicating the chemical coupling between EGCG and M-2070. ^{1}H NMR of J-EGCG was performed to confirm the structure of the Mannich condensate. Figure 2 depicts the ^{1}H NMR spectrum of J-

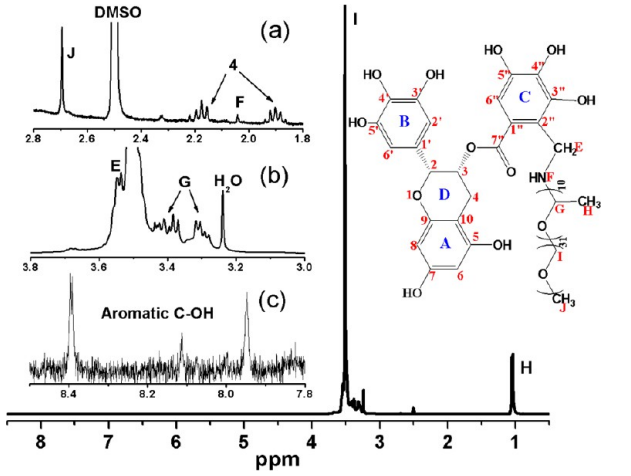

Figure 2. ^{1}H NMR spectrum of JEGCG in DMSO-d_6, the insets are the partial enlarged spectra.

EGCG. Tentative assignments of ^{1}H NMR spectrum of J-EGCG (H-E, -F, -G, -H, -I, -J, -4 and aromatic C−OH at δ_H 3.54 d, 2.32 s, 3.38 m, 1.05 d, 3.51 s, 2.69 s, 2.17 and 8.11 m, respectively) were made by comparison with EGCG from our previous report[23] and literature data.[30,31] Particularly, δ_H at 3.51 represents the H on the methylene in the condensate introduced by formaldehyde. Evidently, the Mannich condensate with a methylene linked structure is confirmed.

Figure 3 is the C 1s XPS spectra of JTPG0, JTPG1, and JTPG2. The XPS C 1s spectra were fitted using Gaussian−Lorentzian functions with a Shirley background correction. In the C 1s spectra, all the samples exhibit four types of carbon of C═C, C−N, C−O, and C═O, corresponding to binding energies at 284.6, 285.2, 286.2, and 287.2 eV, respectively.[32,33] Clearly, the peak area associated with nonconjugated carbon is consistently increased. The sp2 fraction of JTPG0, JTPG1, and JTPG2 are quantitatively calculated as 74.3%, 59.4%, and 53.5%, respectively. The decrease in the sp2 fraction clearly indicates the introduction of polyether by the Mannich reaction. In addition, it can be seen that the peak area for carbon linked to nitrogen (C−N) is increased with the increasing HCHO/M-2070 ratio, suggesting that the Mannich reaction takes place more efficiently with the increase of HCHO content.

The conversion of TPG into JTPG is also characterized using UV−vis spectroscopy. Figure 4 shows the normalized UV−vis absorption spectra of GO, TPG, JTPG, and M-2070 in water. The spectrum of M-2070 shows no obvious absoption in the typical ultraviolet aborption range. GO solution exhibits a maximum at 231 nm and a shoulder at 300 nm, which is ascribed to $\pi-\pi^*$ transitions of aromatic C═C bonds. TPG exhibits an incisive UV absorption peak at 207 nm, characterizing $\pi-\pi^*$ transition of the conjugated structure in benzene from TP.[23] Except for the presence of the peak of 207 nm, TPG solution exhibits a peak at 278 nm and a shoulder at 231 nm, which is ascribed to n-π^* transitions of C═O bonds and $\pi-\pi^*$ transitions of aromatic C═C bonds in TPG, respectively.[34] With the occurred Mannich reaction, it is found that the peak for conjugated structure is red-shifted to 212 nm slowly, which

dx.doi.org/10.1021/am3032822 | ACS Appl. Mater. Interfaces 2013, 5, 2174−2181

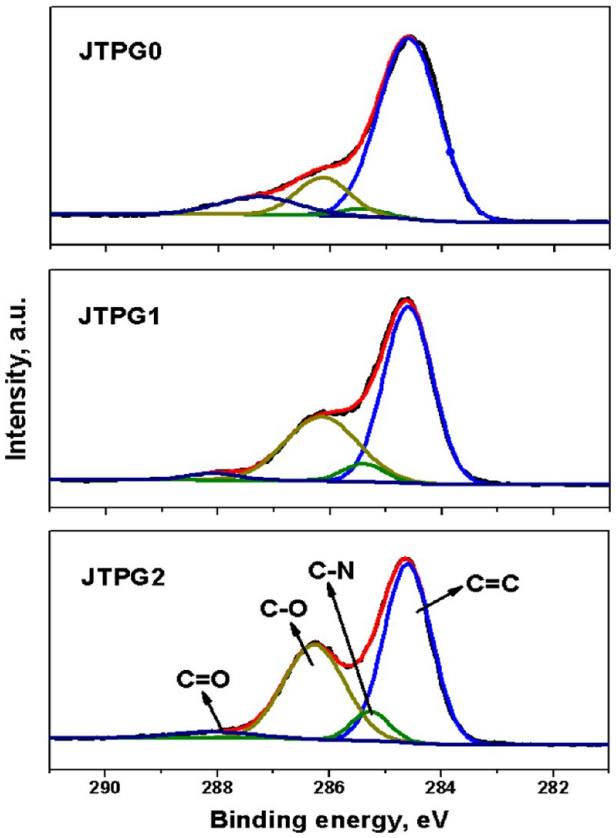

Figure 3. XPS C 1s spectra and peak fittings of JTPG on a silicon wafer substrate.

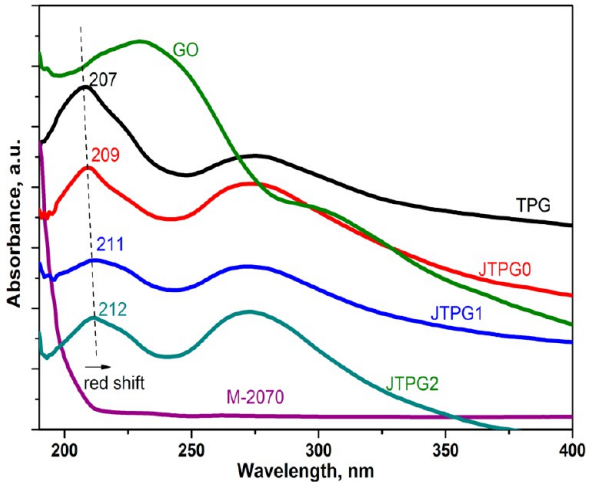

Figure 4. UV−vis spectra of GO, TPG, JTPG, and M-2070.

may be attributed to the effect from the introduced Jeffamine chains.

The organic content and thermal stability of JTPG were evaluated by TGA. The TGA curves of TPG and JTPG samples are shown in Figure 5 (a). Take the residual weight of TPG into account, the grafted M-2070 in JTPG0 is calculated to be about 16.4 wt %. With increasing HCHO, the char yield is consistently decreased, indicating the increasing Mannich condensate on the graphene core. The graphene weight content in JTPG2 is calculated to be about 34.2%. All samples except JTPG2 lose weight below 200 °C, which is mainly due to detachment of some of TP and trace water. Through the Mannich condensation, the molecular weight of the organic portion on the graphene is largely increased, and thus the initial thermal stability is increased. At around 400 °C, the distinct weight loss for JTPG is observed. In contrast to TPG, it is obvious that JTPG exhibits higher thermal stability. As depicted in Figure 5 (b), the maximum decomposition temperature of JTPG is increased from 345 to 377 °C with the increase of HCHO content, which could be attributed to the tethering effect from the graphene core and consequently the thermal cleavage of the chains is restricted.

Solubility and the Microstructure of JTPG. To identify whether JTPG sheets remain separated or become aggregated, observations from AFM and TEM were performed. AFM is currently one of the foremost methods used in definite identification of single-layer graphene.[35] Figure 6 (a, b, c) shows typical AFM images of JTPG sheets in water and the corresponding height profiles. It can be seen that the thickness of JTPG sheets is increased successively from 2.07 to 3.4 nm with the increase of HCHO content. The thickness of JTPG2 is about 3.4 nm, which is much higher than that of TPG (1.4 nm) as revealed previously.[23] The increment in the thickness is attributed to the introduction of M-2070 oligomers on the graphene layer. The variation in the thickness of JTPG is well consistent with XRD result, which will be interpreted later. From the TEM images of JTPG2 (Figure 6 (d, e, f, g)), the layers of JTPG2 dispersed in chloroform, acetone, water, and ethyl acetate are well dispersed as wrinkled silk shapes, a typical feature for the single-layer graphene. In addition, the surface of JTPG is rather smooth in AFM and TEM images, indicating homogeneous coverage of the Mannich condensate on the graphene sheet. The stabilization mechanisms are proposed to be $\pi-\pi$ interactions between the conjugated structures in the Mannich condensate with the graphene layer, together with the hydrogen bonding between the Mannich condensate and the residual oxygenic groups on the graphene layer.[36] Moreover, the capped Mannich condensates supply steric hindrance to stabilize the graphene sheets in solvents.

Figure 7 shows the solubilities of JTPG2 with a fixed concentration of 1.5 mg/mL in water and various organic solvents after one month standing. In the previous study, it has been reported that TPG can only be dispersed in alcohols and some polar organic solvents such as DMF and NMP.[23] In contrast to TPG, as shown in Figure 7, JTPG2 can be stably dispersed in a much wider spectrum of polar solvents including alcohols, esters, ketones, and haloalkanes for more than one month without any precipitation. The stability and colloidal nature of the above solutions of JTPG2 are evidenced by the Tyndall effect. All the diluted dispersions give rise to distinct Tyndall effects, and selected images are also included in Figure 7. However, JTPG2 can only be stably suspended in toluene, butanone, and isopropyl alcohol for several days, implying insufficent stability in these solvents. The excellent stability of JTPG2 in a wide spectrum of polar solvents is attributed to the excellent solubility and miscibility of the Jeffamine chains attached to the graphene sheets. It should be noted that the above-mentioned polar solvents are the solvents with low boiling point and less toxicity. The improvement of the dispersibility of graphene in the solvents with low boiling point and less toxicity is significant as this feature greatly facilitates its practical applications in electronic devices and graphene-based composites.

It should be noted that the most intriguing feature of JTPG is that its production is scalable. First, all the raw materials are at a

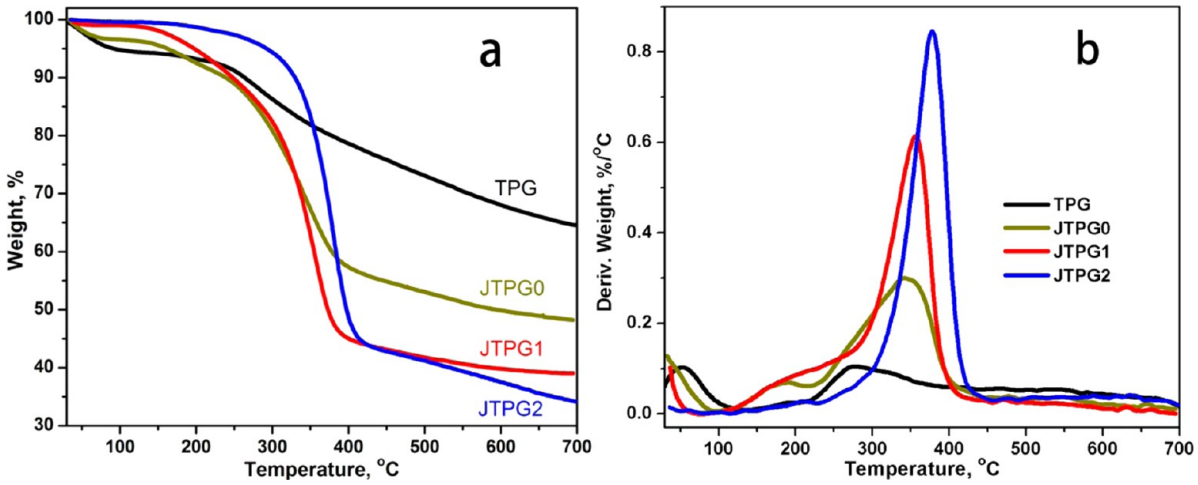

Figure 5. (a) TGA curves and (b) DTG curves of TPG and JTPG.

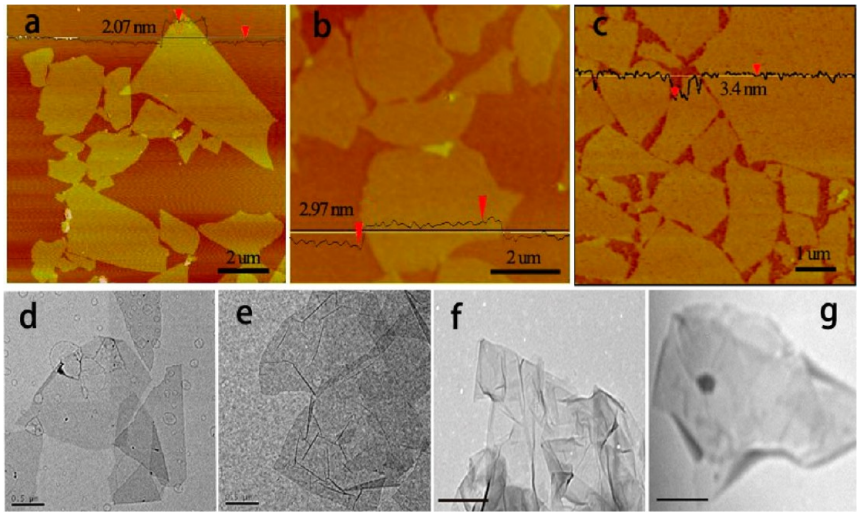

Figure 6. AFM images of (a) JTPG0, (b) JTPG1, and (c) JTPG2 in water; TEM images of JTPG2 in (d) chloroform, (e) acetone, (f) water, and (g) ethyl acetate, the scale bar is 0.5 μm.

low cost and industrially available. Second, the production of JTPG is a one-pot process in water, without a purification step for the intermediates. Moreover, the production of JTPG is actually a facile and energy-saving process as the procedures only include mild heating (5 h @ 80 °C) and centrifugation. Last and most interestingly, the product could exist as slurry form, in which only a small portion of water remains. The slurry exhibits long-term stability during storage. With mild sonication, the slurry could be readily dispersed into excellent dispersion when it is diluted or transported into other organic solvents.

JTPG Hybrid Paper and JTPG-Filled Rubber Composites. For the excellent single-layered dispersity in water and solubility in the broad spectrum of organic solvents, JTPG can be fabricated into tightly packed hybrids through vacuum-assisted filtration. The sideview SEM image of JTPG hybrids (Figure 8) reveals that JTPG layers are intimately stacked into the laminated structure. With a closer eye in Figure 8 (a, b, c), one can found that, with the increase of HCHO content, the laminated structure of JTPG is unambiguously more tight and the graphene sheets are more distinctly found, suggesting the facilitated packing of JTPG layers into the layer-by-layer structure with the addition of HCHO.

The XRD patterns are employed to investigate the microstructures of GO, TPG, and JTPG papers, as illustrated in Figure 8 (d, e). The characteristic diffraction peak of GO appears at 9.7°, and its interlayer distance is 0.91 nm according to the Bragg equation. In the XRD pattern of TPG, the diffraction peak at 25.32° (*d*-spacing of 0.35 nm) is related to the interlayer distance between TP and graphene. The diffraction peak at 4.63° (*d*-spacing of 1.9 nm) is attributed to the interlayer distance between two adjacent graphene layers which sandwichs TP molecules.[23] Upon the Mannich reaction, the (*002*) peak shifts to a lower angle around 22.13° (*d*-spacing of 0.41 nm). This increase in *d*-spacing is due to the generation and intercalation of Mannich condensate molecules. The interlayer distance between two adjacent grahene layers is calculated to be increasing with the addition of HCHO, which is also due to the introduction of the Mannich condensate with higher molecular weight into the adjacent graphene layers. As such, the interlayer distance of JTPG2 is ~3.54 nm, which is nearly identical to the value (~3.4 nm) obtained from the AFM result (Figure 6 (c)). This result provides further implication of the face-on arrangement of the Mannich condensate molecules on both sides of the TPG sheet.

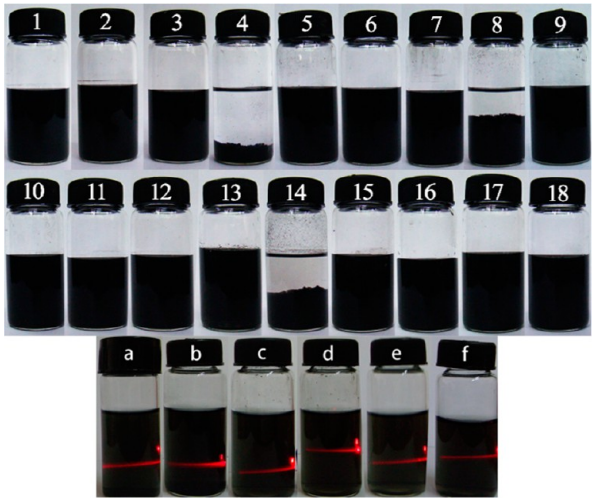

Figure 7. Photographs of JTPG2 dispersions (1.5 mg/mL) one month after sonication in 1) methyl methacrylate, 2) methyl acrylate, 3) ethyl acetate, 4) toluene, 5) dichloromethane, 6) chloroform, 7) acetone, 8) butanone, 9) DMSO, 10) THF, 11) methanol, 12) ethanol, 13) ethylene glycol, 14) isopropyl alcohol, 15) propanediol, 16) DMF, 17) NMP, and 18) water and selected Tyndall effects in (a) ethyl acetate, (b) dichloromethane, (c) acetone, (d) THF, (e) ethanol, and (f) water.

Raman spectroscopy was used to further characterize the structure of JTPG. Figure 9 shows the Raman spectra of TPG and JTPG with different HCHO content. It can be seen that TPG and JTPG exhibit a D band around 1327 cm^{-1}, which is induced by their disordered structure or sp^3 hybridized carbons. The G band, which is derived from the splitting of the E_{2g} stretching mode of graphite or the in-plane bonding stretching motion of pairs of sp^2 C atoms, is also observed. Usually, the intensity ratio of the D band and the G band (I_D/I_G) is used to characterize the defects and monitor the functionalization of carbonaceous materials. In the present work, compared with TPG, the value of I_D/I_G for JTPG is increased. This can be explained by the increasing new edges introduced during the Mannich reaction and provides additional clues for the functionalization of TPG. With the increase of HCHO content, the organic fraction on graphene is consistently increased. The introduced polyether oligomer facilitates the packing of graphene layers which have be substantiated by the SEM evidence. Consequently, with the increase of HCHO content,

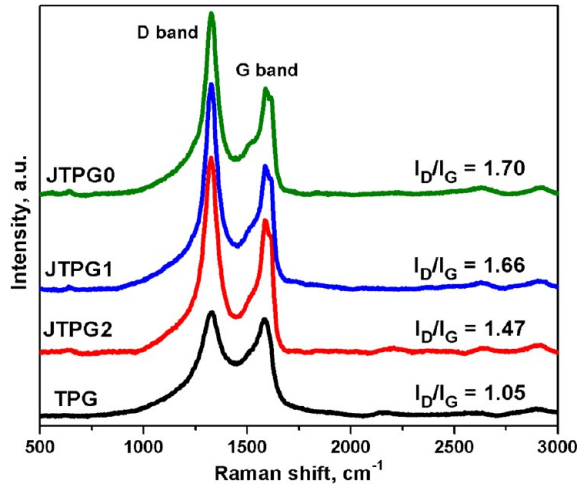

Figure 9. Raman spectra of TPG and JTPG.

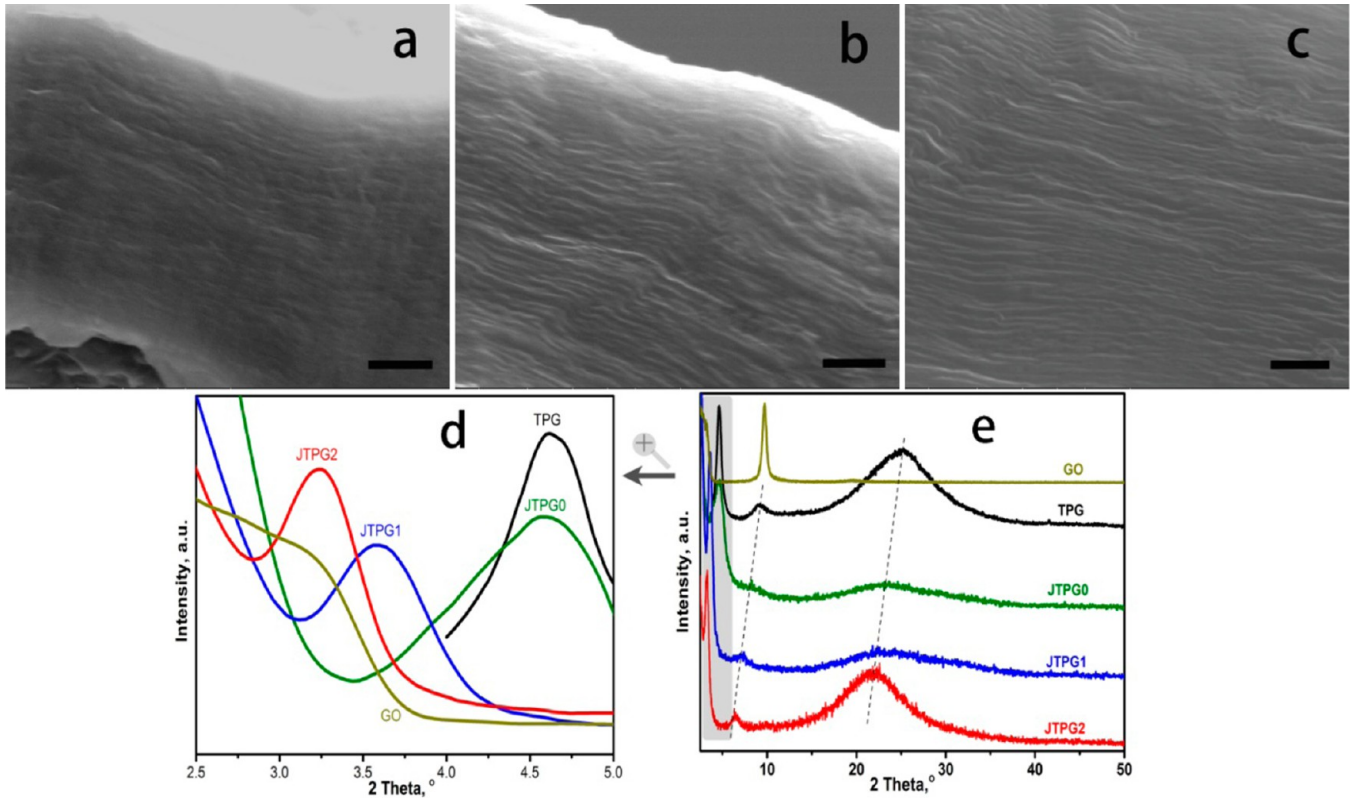

Figure 8. Side-view SEM images of (a) JTPG0, (b) JTPG1, (c) JTPG2, the scale bar is 1 um; (d) and (e): XRD patterns of GO, TPG, and JTPG.

dx.doi.org/10.1021/am3032822 | ACS Appl. Mater. Interfaces 2013, 5, 2174−2181

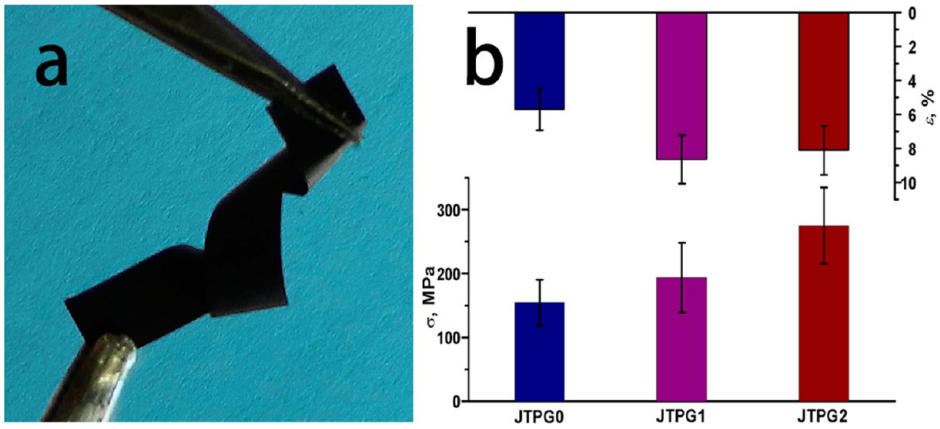

Figure 10. (a) Twisted JTPG2 paper and (b) the tensile property of JTPG.

the ordering of the graphene layers is increased, and the I_D/I_G value is decreased.

The two-dimensional structure of the graphene sheet makes it easy to assemble into paper-like materials through simple filtration[37] or liquid/air interface self-assembly.[38] Previous studies showed that the macroscopic graphene papers exhibited the impressive strength (76−293 MPs) and modulus (6−42 GPa), which surpass most of the other paper-like materials such as buckypaper or vermiculite paper.[39,40] The mechanical properties of the GO or graphene papers can be further improved by introducing chemical cross-link between adjacent graphene sheets using divalent ions[41] or polyallylamine.[42] However, the reported graphene papers are brittle with ultimate strain less than 1%, which hampers their applications. The flexible JTPG hybrids (Figure 10 (a)) exhibit extraordinarily strong mechanical property. The tensile strength and elongation of JTPG papers are found to be dependent on the HCHO content. As shown in Figure 10 (b), JTPG2 paper possesses the maximum averaged strength of 275 MPa. Particularly, JTPG2 paper exhibits ultimate strain as large as 8%, which is much higher than those for the reported graphene paper (0.2−0.8%).[43,44] That is, in contrast to the generally brittle graphene papers,[44−46] JTPG papers are robust yet tough. The combination of high strength and high toughness for JTPG papers may be attributed to the four aspects below. First, in the present study, JTPG possesses a well restored sp2 structure and aspect ratio which are crucial to its high strength and reinforcing capability. Second, JTPG papers possess high graphene content (as high as 34.2%), which is the key point for gaining high strength of the hybrid. Third, graphene layers pack tightly through the entanglement of Jeffamine chains. In addition, the interfacial cross-linking may be generated to some extent during the drying of the JTPG papers. These outcomes make effective stress-transferring among the graphene layers upon loading. Finally, the interaction force between graphene layers is mainly noncovalent forces. When the load is applied, the graphene layer can slippage against the adjacents layer by untangling the Jeffamine chains. Consequently the JTPG papers exhibit exceptional toughness. As we indicated above, the graphene layers reduced by polyphenols possess good quality of the conjugated structure. With the introduction of Jeffamine, graphene layers are packed tightly during the preparation, which permits the interconnection among the graphene layers. As a consequence, the JTPG hybrid still possesses fairly high electrial conductivity (~700 S/m for JTPG2). Therefore, the heterogeneous hybrids film with individually dispersed graphene sheets in a matrix of the Mannich condensate is expected to find potential applications in which the combination of high strength and electrical conductivity is essential.

Due to the excellent solubility of JTPG, the composite consisting JTPG could also be facilely fabricated by the solution compounding in the solvent with low boiling point and low toxicity. Herein, NBR was used as an example to illustrate the potential of JTPG in increasing conductivity of polymer. As depicted in Figure 11, the electrical conductivity of the NBR/

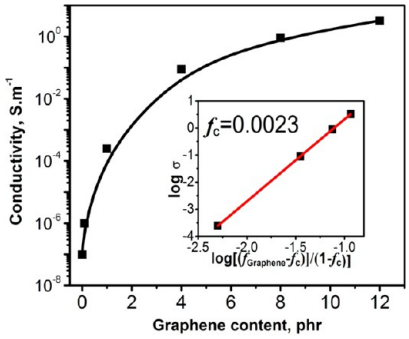

Figure 11. Evolution of electrical conductivity of NBR/JTPG composite. The inset is the logarithmic plot for conductivity versus $(f_{Graphene} - f_c)/(1 - f_c)$. The linear fit is done using power laws.[47] f_c and $f_{Graphene}$ represent the percolation threshold and graphene volume fraction in the composites, respectively.

JTPG composite is increased consistently with increasing JTPG content. In addition, the calculated threshold percolation is as low as 0.23 vol.% of graphene. The graphene contents in the composites are calculated based on the graphene content in JTPG2 (about 34.2%). The impressive low percolation threshold suggests the effective formation of a conductivity pathway, possibly due to the excellent compatibility of the Mannich condensate with NBR. Thus, it is explicit that JTPG has the promising potential in fabrication of functional polymer composites with low threshold percolation.

CONCLUSION

Through a facile and one-pot process, a kind of amphiphilic graphene (JTPG) could be fabricated through the reduction of GO with tea polyphenols and subsequent Mannich condensation between the polyphenols and a monofunctional polyetheramine (Jeffamine M-2070). Due to the utilization of

industrially available raw materials and the short-term one-pot process, the fabrication of JTPG is demonstrated to be scalable and cost-effective. JTPG shows excellent solubility and stability in a wide spectrum of solvents, including water and the solvents with low boiling point and low toxicity. JTPG paper prepared by vacuum assisted filtration exhibits an unusual combination of high toughness (tensile strength of ~275 MPa and break strain of ~8%) and electrical conductivity (~700 S/m). In addition, due to the excellent solubility in the solvents with low boiling point and low toxicity, JTPG is also promising in the fabrication of polymer/graphene composites with high performance. For instance, nitrile rubber (NBR)/JTPG composites are fabricated by the solution compounding in acetone. The resulting composite exhibits low threshold percolation at 0.23 vol.% of graphene. The versatilities in dispersibility and performance, together with the scalable process of JTPG, enable a new way to scale up the fabrication for the graphene-based polymer composites or hybrids with high performance.

AUTHOR INFORMATION

Corresponding Author

*E-mail: psbcguo@scut.edu.cn.

Notes

The authors declare no competing financial interest.

ACKNOWLEDGMENTS

This work was supported by National Natural Science Foundation of China (51222301 and 50933001), Program for New Century Excellent Talents in University (NCET-10-508 0393), Fundamental Research Project for the Central Universities (2012ZG0002) and Key Technologies R&D Program of Guangzhou City.

REFERENCES

(1) Edwards, R. S.; Coleman, K. S. *Nanoscale* **2013**, *5*, 38−51.
(2) Luo, B.; Liu, S.; Zhi, L. *Small* **2012**, *8*, 630−646.
(3) Batzill, M. *Surf. Sci. Rep.* **2012**, *67*, 83−115.
(4) Rao, C. N. R.; Sood, A. K.; Subrahmanyam, K. S.; Govindaraj, A. *Angew. Chem., Int. Ed.* **2009**, *48*, 7752−7777.
(5) Weiss, N. O.; Zhou, H.; Liao, L.; Liu, Y.; Jiang, S.; Huang, Y.; Duan, X. *Adv. Mater.* **2012**, *24*, 5782−5825.
(6) Potts, J. R.; Dreyer, D. R.; Bielawski, C. W.; Ruoff, R. S. *Polymer* **2011**, *52*, 5−25.
(7) Georgakilas, V.; Otyepka, M.; Bourlinos, A. B.; Chandra, V.; Kim, N.; Kemp, K. C.; Hobza, P.; Zboril, R.; Kim, K. S. *Chem. Rev.* **2012**, *112*, 6156−6214.
(8) Niyogi, S.; Bekyarova, E.; Itkis, M. E.; Zhang, H.; Shepperd, K.; Hicks, J.; Sprinkle, M.; Berger, C.; Lau, C. N.; Deheer, W. A. *Nano Lett.* **2010**, *10*, 4061−4066.
(9) Shan, C.; Yang, H.; Han, D.; Zhang, Q.; Ivaska, A.; Niu, L. *Langmuir* **2009**, *25*, 12030−12033.
(10) Xu, Y.; Liu, Z.; Zhang, X.; Wang, Y.; Tian, J.; Huang, Y.; Ma, Y.; Chen, Y. *Adv. Mater.* **2009**, *21*, 1275−1279.
(11) Yang, H.; Shan, C.; Li, F.; Han, D.; Zhang, Q.; Niu, L. *Chem. Commun.* **2009**, 3880−3882.
(12) Yang, H.; Li, F.; Shan, C.; Han, D.; Zhang, Q.; Niu, L.; Ivaska, A. *J. Mater. Chem.* **2009**, *19*, 4632−4638.
(13) Colson, J. W.; Woll, A. R.; Mukherjee, A.; Levendorf, M. P.; Spitler, E. L.; Shields, V. B.; Spencer, M. G.; Park, J.; Dichtel, W. R. *Science* **2011**, *332*, 228−231.
(14) Reuven, D.; Li, H.; Harruna, I.; Wang, X.-Q. *J. Mater. Chem.* **2012**, *22*, 15689−15694.
(15) Reuven, D. G.; Suggs, K.; Williams, M. D.; Wang, X.-Q. *ACS Nano* **2012**, *6*, 1011−1017.
(16) Zhang, S.; Shao, Y.; Liao, H.; Engelhard, M. H.; Yin, G.; Lin, Y. *ACS Nano* **2011**, *5*, 1785−1791.
(17) Xu, Y. X.; Bai, H.; Lu, G. W.; Li, C.; Shi, G. Q. *J. Am. Chem. Soc.* **2008**, *130*, 5856−5857.
(18) Tang, Z.; Zeng, C.; Lei, Y.; Guo, B.; Zhang, L.; Jia, D. *J. Mater. Chem.* **2011**, *21*, 17111−17118.
(19) Tang, Z.; Lei, Y.; Guo, B.; Zhang, L.; Jia, D. *Polymer* **2011**, *53*, 673−680.
(20) Kozhemyakina, N. V.; Englert, J. M.; Yang, G.; Spiecker, E.; Schmidt, C. D.; Hauke, F.; Hirsch, A. *Adv. Mater.* **2010**, *22*, 5483−5487.
(21) Zhang, Y.; Mori, T.; Niu, L.; Ye, J. *Energy Environ. Sci.* **2011**, *4*, 4517−4521.
(22) Bai, H.; Xu, Y.; Zhao, L.; Li, C.; Shi, G. *Chem. Commun.* **2009**, 1667−1669.
(23) Liao, R.; Tang, Z.; Lei, Y.; Guo, B. *J. Phys. Chem. C* **2011**, *115*, 20740−20746.
(24) Wang, Y.; Shi, Z. X.; Yin, J. *ACS Appl. Mater. Interfaces* **2011**, *3*, 1127−1133.
(25) Hummers, W. S., Jr.; Offeman, R. E. *J. Am. Chem. Soc.* **1958**, *80*, 1339−1339.
(26) Wu, H.; Huang, X.; Gao, M.; Liao, X.; Shi, B. *Green Chem.* **2011**, *13*, 651−658.
(27) Zhu, H.; Du, M. L.; Zou, M. L.; Xu, C. S.; Fu, Y. Q. *Dalton Trans.* **2012**, *41*, 10465−10471.
(28) Bors, W.; Michel, C.; Stettmaier, K. *Arch. Biochem. Biophys.* **2000**, *374*, 347−355.
(29) Wang, G.; Shen, X.; Wang, B.; Yao, J.; Park, J. *Carbon* **2009**, *47*, 1359−1364.
(30) Mladenova, R.; Ignatova, M.; Manolova, N.; Petrova, T.; Rashkov, I. *Eur. Polym. J.* **2002**, *38*, 989−999.
(31) Laobuthee, A.; Chirachanchai, S.; Ishida, H.; Tashiro, K. *J. Am. Chem. Soc.* **2001**, *123*, 9947−9955.
(32) Sundberg, P.; Larsson, R.; Folkesson, B. *J. Electron Spectrosc. Relat. Phenom.* **1988**, *46*, 19−29.
(33) Stankovich, S.; Dikin, D. A.; Piner, R. D.; Kohlhaas, K. A.; Kleinhammes, A.; Jia, Y.; Wu, Y.; Nguyen, S. B. T.; Ruoff, R. S. *Carbon* **2007**, *45*, 1558−1565.
(34) Wang, L.; Liao, R.; Tang, Z.; Lei, Y.; Guo, B. *J. Phys. D: Appl. Phys.* **2011**, *44*, 445302.
(35) Kuila, T.; Bose, S.; Mishra, A. K.; Khanra, P.; Kim, N. H.; Lee, J. H. *Prog. Mater. Sci.* **2012**, *57*, 1061−1105.
(36) Lei, Y.; Tang, Z.; Liao, R.; Guo, B. *Green Chem.* **2011**, *13*, 1655−1658.
(37) Dikin, D. A.; Stankovich, S.; Zimney, E. J.; Piner, R. D.; Dommett, G. H. B.; Evmenenko, G.; Nguyen, S. T.; Ruoff, R. S. *Nature* **2007**, *448*, 457−460.
(38) Chen, C.; Yang, Q. H.; Yang, Y.; Lv, W.; Wen, Y.; Hou, P. X.; Wang, M.; Cheng, H. M. *Adv. Mater.* **2009**, *21*, 3007−3011.
(39) Gao, Y.; Liu, L. Q.; Zu, S. Z.; Peng, K.; Zhou, D.; Han, B. H.; Zhang, Z. *ACS Nano* **2011**, *5*, 2134−2141.
(40) Chen, H.; Muller, M. B.; Gilmore, K. J.; Wallace, G. G.; Li, D. *Adv. Mater.* **2008**, *20*, 3557−3561.
(41) Park, S.; Lee, K. S.; Bozoklu, G.; Cai, W.; Nguyen, S. T.; Ruoff, R. S. *ACS Nano* **2008**, *2*, 572−578.
(42) Park, S.; Dikin, D. A.; Nguyen, S. T.; Ruoff, R. S. *J. Phys. Chem. C* **2009**, *113*, 15801−15804.
(43) Park, S.; Mohanty, N.; Suk, J. W.; Nagaraja, A.; An, J.; Piner, R. D.; Cai, W.; Dreyer, D. R.; Berry, V.; Ruoff, R. S. *Adv. Mater.* **2010**, *22*, 1736−1740.
(44) Chen, H.; Müller, M. B.; Gilmore, K. J.; Wallace, G. G.; Li, D. *Adv. Mater.* **2008**, *20*, 3557−3561.
(45) Park, S.; Lee, K. S.; Bozoklu, G.; Cai, W.; Nguyen, S. B. T.; Ruoff, R. S. *ACS Nano* **2008**, *2*, 572−578.
(46) Dikin, D. A.; Stankovich, S.; Zimney, E. J.; Piner, R. D.; Dommett, G. H. B.; Evmenenko, G.; Nguyen, S. B. T.; Ruoff, R. S. *Nature* **2007**, *448*, 457−460.
(47) Dang, Z. M.; Wang, L.; Yin, Y.; Zhang, Q. *Adv. Mater.* **2007**, *19*, 852−857.